

# Transient VRM Response From a Large Circular Loop Over a Conductive and Magnetically Viscous Half-Space

Devin C. Cowan, *Student Member, IEEE*, Lin-Ping Song, *Member, IEEE*, and Douglas W. Oldenburg

**Abstract**—To effectively characterize the impact of viscous remanent magnetization (VRM) on the transient electromagnetic response, we present a set of analytical expressions for the vertical and radial VRM responses generated by a large circular loop over a magnetically viscous half-space. For a step-off excitation, Néel relaxation theory is used to express the VRM within the half-space as the product of a static on-time magnetization and a time-dependent aftereffect function. Through heuristic and empirical approximations to the elliptic integral of the second kind, we are able to convert Hankel integral-based expressions for static fields into simplified analytical expressions. These were validated with a numerical 1-D forward modeling code. Analytical expressions show that VRM responses are largest near the transmitter wire, and that at the center of a large loop, the strength of the VRM response is inversely proportional to the loop's radius. We also present an estimate of the crossover time from which the VRM signal starts to dominate the transient response. We found that later crossover times were observed near the centers of large loops and that crossover times were much earlier near the transmitter wire. Also, the magnetic flux density has an earlier crossover time compared with its time derivative. To lower or remove the VRM response in an anticipated survey, our analytical expressions can be used straightforwardly to choose an appropriate loop size, identify the VRM response time window, and select an optimal set of time channels.

**Index Terms**—Circular loop, crossover time, inductive response, magnetic soil, time-domain electromagnetic (TEM) systems, viscous remanent magnetization (VRM).

## I. INTRODUCTION

MANY inductive source time-domain electromagnetic (TEM) systems use a step-offlike excitation to measure the response from a desired target. In lateritic soils, sudden removal of the transmitter's primary field induces a time-dependent magnetic relaxation due to the presence of superparamagnetic (SP) iron-oxide grains [1]–[5]. This magnetic relaxation process is known as viscous remanent magnetization (VRM), magnetic viscosity, or magnetic aftereffect [6]–[8]. The VRM experienced by a lateritic soil generates a distinct transient response from that of a nonmagnetic conductive soil. This response, termed the VRM response, can

severely contaminate the TEM responses from conductive ore bodies and unexploded ordnance items when lateritic soils are prominent [1]–[5], [9]. Thus, to properly account for the VRM signal in a set of TEM data, it is of practical interest to first understand the behaviors of the VRM response.

Over the past decades, studies have been done to characterize the VRM responses exhibited by magnetically viscous soils [1]–[5], [9], [12]. It is well known that the induced voltage within a receiver coil due to the VRM response has a  $1/t$  decay, where  $t$  is the time. Through experimental, analytical, and numerical means, researchers have also shown that measured VRM responses can be diminished by: separating the receiver from the transmitter, increasing the size of the transmitter loop, or elevating the sensor further above the ground [1], [2], [5], [11], [13], [14]. Despite providing significant insight, some details regarding the VRM response and its computation appear elusive. Existing numerical and analytical methods [2]–[4], [10], [11], [13]–[15] are both complicated and lack sufficient insight regarding the quantitative dependence of the VRM response on the survey geometry. In addition, the current understanding of the VRM response is mainly drawn from the vertical component. With the increasing development of advanced triaxial TEM sensors, characterizing the radial VRM response is another necessary and desirable aspect.

In this paper, we attempt to fill gaps left in previous studies of the VRM response. We consider a circular transmitter loop over a magnetically viscous half-space and derive simplified analytical expressions for the vertical and horizontal components of the VRM response. Both the magnetic flux and its time derivative are considered for several survey configurations. With the set of new formulas, we are able to effectively model the transient VRM response directly as a function of the survey's geometric properties and predict the times when the VRM signal dominates the TEM response. As a result, quantitative information can easily be obtained to characterize the amplitude and time range of transient VRM responses.

The remainder of this paper is organized as follows. In Section II, we review Néel relaxation theory in the frequency and time domain. General formulation of the VRM response is briefly presented in Section III. In Section IV, we derive the analytical expressions for vertical and radial static magnetic fields over an SP half-space. These are used to predict the VRM response in Section V, where final analytical

Manuscript received November 27, 2015; revised July 15, 2016 and December 6, 2016; accepted February 1, 2017. (*Corresponding author: Devin C. Cowan.*)

The authors are with the Department of Earth, Ocean and Atmospheric Sciences, The University of British Columbia, Vancouver, BC V6T 1Z4, Canada (e-mail: devinccowan@gmail.com).

Color versions of one or more of the figures in this paper are available online at <http://ieeexplore.ieee.org>.

Digital Object Identifier 10.1109/TGRS.2017.2675406

expressions are validated using a 1-D numerical modeling code. In Section VI, we inspect the separability of inductive and VRM responses over a conductive and magnetically viscous half-space and present the analytical formulas to estimate the crossover time. Section VII concludes this paper.

## II. MAGNETIC VISCOSITY IN LATERITIC SOILS: A REVIEW OF NÉEL RELAXATION THEORY

The magnetic viscosity observed in lateritic soils is commonly understood using thermal relaxation models [7] for a collection of noninteracting SP single-domain grains [1], [3], [4], [6], [8], [12]. In this section, we present mathematical expressions derived by Néel [7] that will be used later to predict the VRM response for a half-space.

### A. Frequency-Dependent Magnetic Susceptibility

Magnetic susceptibility relates the induced magnetization  $\vec{M}(\omega)$  to the applied magnetic field  $\vec{H}(\omega)$ . For lateritic soils, the magnetic susceptibility can be frequency-dependent [6], [11], [19]

$$\vec{M}(\omega) = \chi(\omega)\vec{H}(\omega). \quad (1)$$

By assuming that all SP grains are identical, the frequency-dependent magnetic susceptibility for a theoretical sample can be expressed using a Debye model [4], [6], [20]

$$\chi(\omega) = \chi_\infty + \frac{\Delta\chi}{1 + i\omega\tau} \quad (2)$$

where  $\tau$  is the time-relaxation constant for the collection of SP grains,  $\Delta\chi$  represents the variation in magnetic susceptibility over  $\omega \in [0, \infty]$  due to VRM, and  $\chi_\infty$  is the susceptibility representing instantaneous magnetization within the sample. The time-relaxation constant for the sample is given by [7]

$$\tau = \tau_0 \exp\left(\frac{E_b}{k_B T}\right) \quad (3)$$

where  $k_B$  is the Boltzmann constant,  $T$  is the absolute temperature, and  $\tau_0 \sim 10^{-9}$  s is the ‘‘attempt time.’’  $E_b$  represents the energy barriers that maintain the preexisting orientations of individual SP grains. In natural soils,  $E_b$  is not the same for all SP grains, and instead forms a distribution. By (3), lateritic soils are characterized by a distribution of time-relaxation constants that is represented using a weighting function  $f(\tau)$ . Applying the weighting function and integrating over all Debye models (2), the soil’s magnetic susceptibility is expressed as [4], [6], [20]

$$\chi(\omega) = \chi_\infty + \Delta\chi \int_0^\infty \frac{f(\tau)}{1 + i\omega\tau} d\tau. \quad (4)$$

The majority of lateritic soil samples can be adequately fit by assuming a log-uniform distribution of time-relaxation constants between a set of finite limits  $[\tau_1, \tau_2]$  [6], [20]–[22]. The weighting function for a log-uniform distribution of time-relaxation constants is defined by [3], [6], [14], [20]

$$f(\tau) = \begin{cases} \frac{1}{\tau \ln(\tau_2/\tau_1)} & \text{for } \tau_1 \leq \tau \leq \tau_2 \\ 0 & \text{otherwise.} \end{cases} \quad (5)$$

Substituting (5) into (4), we obtain

$$\begin{aligned} \chi(\omega) &= \chi_\infty + \frac{\Delta\chi}{\ln(\tau_2/\tau_1)} \int_{\tau_1}^{\tau_2} \frac{1}{\tau(1 + i\omega\tau)} d\tau \\ &= \chi_\infty + \Delta\chi \left[ 1 - \frac{1}{\ln(\tau_2/\tau_1)} \ln\left(\frac{1 + i\omega\tau_2}{1 + i\omega\tau_1}\right) \right]. \end{aligned} \quad (6)$$

Equation (6) represents an appropriate frequency-dependent magnetic susceptibility model that can be used to characterize most lateritic soils [4], [6], [11], [20], [21]. This model is used to characterize magnetic viscosity in the 1-D numerical modeling code [18]. It is easy to show, from (6), that  $\chi(\omega \rightarrow 0) = \chi_\infty + \Delta\chi$ , and that  $\chi(\omega \rightarrow \infty) = \chi_\infty$ . Thus,  $\Delta\chi$  represents the static magnetic susceptibility for the collection of SP grains. In this paper,  $\chi_\infty$  will not play any significant role when predicting the soil’s response as observations will be made during the off-time.

### B. Viscous Remanent Magnetization in Response to Step-Off Excitation

Consider a step-off excitation where a dc field  $\vec{H}_0$ , which has been applied to a magnetically viscous sample since  $t = -\infty$ , is suddenly removed at  $t = 0$ . In this case, the resulting magnetic relaxation at  $t > 0$  can be expressed as [3], [4], [7]

$$\vec{M}(t) = \Delta\chi \vec{H}_0 F(t) \quad (7)$$

where  $F(t)$  is referred to as the aftereffect function. If all SP grains are characterized by an identical time-relaxation constant  $\tau$ , then the aftereffect function is given by [3], [4], [7]

$$F(t) = e^{-t/\tau}. \quad (8)$$

For a distribution of time-relaxation constants, (8) becomes [3], [4], [7], [20]

$$F(t) = \int_0^\infty f(\tau) e^{-t/\tau} d\tau \quad (9)$$

where  $f(\tau)$  is the weighting function defined in (4). For a soil characterized by a log-uniform distribution of time-relaxation constants, substituting (5) into (9) leads to

$$\begin{aligned} F(t) &= \frac{1}{\ln(\tau_2/\tau_1)} \int_{\tau_1}^{\tau_2} \frac{1}{\tau} e^{-t/\tau} d\tau \\ &= \frac{1}{\ln(\tau_2/\tau_1)} \left[ Ei\left(\frac{t}{\tau_2}\right) - Ei\left(\frac{t}{\tau_1}\right) \right] \end{aligned} \quad (10)$$

where  $Ei$  is the exponential integral function. When observations are made at time  $\tau_1 \ll t \ll \tau_2$ ,  $Ei(t/\tau_1) \approx 0$  and  $Ei(t/\tau_2) \approx -\gamma - \ln(t/\tau_2)$ , where  $\gamma \approx 0.5772$  is the Euler constant [4]. Over this time period, the aftereffect function can be approximated by

$$F(t) \approx \bar{F}(t) = \frac{1}{\ln(\tau_2/\tau_1)} [-\gamma - \ln(t) + \ln(\tau_2)]. \quad (11)$$

By taking the derivative of (10), we obtain

$$\begin{aligned} \frac{dF(t)}{dt} &= \frac{1}{\ln(\tau_2/\tau_1)} \int_{\tau_1}^{\tau_2} -\frac{1}{\tau^2} e^{-t/\tau} d\tau \\ &= \frac{1}{\ln(\tau_2/\tau_1)} \left[ \frac{e^{-t/\tau_1} - e^{-t/\tau_2}}{t} \right]. \end{aligned} \quad (12)$$

At time  $\tau_1 \ll t \ll \tau_2$ , (12) simplifies to the following expression:

$$\frac{dF(t)}{dt} \approx \frac{d\bar{F}(t)}{dt} = -\frac{1}{\ln(\tau_2/\tau_1)} \frac{1}{t}. \quad (13)$$

We see that (11) and (13) describe the transient VRM and its time derivative as decaying proportional to  $\ln(t)$  and  $1/t$  for  $\tau_1 \ll t \ll \tau_2$ , respectively. The  $1/t$  dependence is often observed in magnetic soil environments when  $\partial B/\partial t$  is being measured [1], [4], [6]. In Sections IV–VI, both approximate time functions will be used to derive the expressions, which characterize the VRM of our half-space to step-off excitation.

### III. GENERAL FORMULATION OF THE VRM RESPONSE IN THE ABSENCE OF SELF-DEMAGNETIZATION

In the absence of self-demagnetization, the magnetic anomaly observed outside a magnetized body can be expressed using the following dyadic Green's function [23]:

$$\vec{B}(\vec{r}, t) = \frac{\mu_0}{4\pi} \int_V \nabla \nabla \frac{1}{|\vec{r} - \vec{r}_s|} \cdot \vec{M}(\vec{r}_s, t) dV_s \quad (14)$$

where  $r$  is the location of observation,  $r_s$  are locations within the volume being integrated, and  $t$  represents time.

For a step-off excitation, we can use (7) to represent the total magnetization at any location within a magnetically viscous Earth at  $t > 0$ . This is because any instantaneous magnetization attributed to  $\chi_\infty$  is zero during the off-time. In most cases, we can expect  $\Delta\chi(\vec{r}_s)$  and the inducing field  $\vec{H}_0(\vec{r}_s)$  to vary spatially. If the spatial distribution of time-relaxation constants defined in expression (5) is uniform everywhere within the magnetically viscous Earth, the aftereffect function  $F(t)$  is spatially invariant and can be taken outside of the integral in (14), which becomes

$$\begin{aligned} \vec{B}(\vec{r}, t) &= \frac{\mu_0}{4\pi} F(t) \int_V \nabla \nabla \frac{1}{|\vec{r} - \vec{r}_s|} \cdot \Delta\chi(\vec{r}_s) \vec{H}_0(\vec{r}_s) dV \\ &= \vec{B}^{(0)}(\vec{r}) F(t) \end{aligned} \quad (15)$$

where  $\vec{B}^{(0)}(\vec{r})$  defines the static magnetic response of all SP grains.

By taking the derivative of (15)

$$\begin{aligned} \frac{\partial \vec{B}(\vec{r}, t)}{\partial t} &= \frac{\mu_0}{4\pi} \frac{dF(t)}{dt} \int_V \nabla \nabla \frac{1}{|\vec{r} - \vec{r}_s|} \cdot \Delta\chi(\vec{r}_s) \vec{H}_0(\vec{r}_s) dV \\ &= \vec{B}^{(0)}(\vec{r}) \frac{dF(t)}{dt}. \end{aligned} \quad (16)$$

Thus, if  $\vec{B}^{(0)}(\vec{r})$  is known, the pairs of (10) and (15), and (12) and (16) can be used to predict  $\vec{B}(\vec{r}, t)$  and  $(\partial \vec{B}(\vec{r}, t)/(\partial t))$  for the VRM response at  $t > 0$ . Next, we present analytic expressions for  $\vec{B}^{(0)}(\vec{r})$ .

### IV. DERIVING THE STATIC MAGNETIC FIELDS OVER A SUPERPARAMAGNETIC HALF-SPACE

We consider an SP half-space in which  $\chi_\infty = 0$  in (6). According to [24, eqs. (4.87) and (4.88)], for a circular transmitter loop with a radius of  $a$  and at height  $h$  above

the surface, vertical and radial components of  $\vec{B}^{(0)}(\vec{r})$  can be obtained by taking their limits as  $\omega \rightarrow 0$ , that is

$$\begin{aligned} B_z^{(0)}(\rho, z) &= \frac{\mu_0 I a}{2} \left( \frac{\Delta\chi}{2 + \Delta\chi} \right) \\ &\times \int_0^\infty \lambda e^{-\lambda(z+h)} J_1(\lambda a) J_0(\lambda \rho) d\lambda \end{aligned} \quad (17)$$

and

$$\begin{aligned} B_\rho^{(0)}(\rho, z) &= -\frac{\mu_0 I a}{2} \left( \frac{\Delta\chi}{2 + \Delta\chi} \right) \\ &\times \int_0^\infty \lambda e^{-\lambda(z+h)} J_1(\lambda a) J_1(\lambda \rho) d\lambda \end{aligned} \quad (18)$$

where  $I$  is the steady-state current,  $\Delta\chi$  is the static magnetic susceptibility due to the SP effects of the half-space,  $\mu_0 = 4\pi \times 10^{-7}$  H/m is the permeability of free space,  $\rho$  is the radial distance from the loop's center axis, and  $z$  is the observation height above the surface.  $J_0(\cdot)$  and  $J_1(\cdot)$  are the zeroth- and the first-order Bessel functions of the first kind, respectively. Note that we are neglecting the primary field contributions for equations found in [24].

We see that even for the static case, the vertical and radial components of  $\vec{B}^{(0)}(\vec{r})$  involve solutions to complicated Hankel transforms in (17) and (18). Their general solutions have to be obtained via numerical integrations [29], [30]. However, for several cases of interest considered in Sections IV-A and IV-B, we can derive analytic solutions or approximate solutions for both the vertical component  $B_z(\rho, z)$  and radial component  $B_\rho(\rho, z)$ .

#### A. Vertical Static Response for a Circular Transmitter Loop Over a Superparamagnetic Half-Space

To solve the integral in (17), we introduce the following identity [25]:

$$\begin{aligned} \int_0^\infty \lambda e^{-\lambda(z+h)} J_1(\lambda a) J_0(\lambda \rho) d\lambda \\ = \frac{a}{\pi} \int_0^\pi [(z+h+i\rho \cos \phi)^2 + a^2]^{-3/2} d\phi. \end{aligned} \quad (19)$$

A general analytical solution to (19) is difficult to derive. For several special cases, however, working with the right-hand side of the equation enables us to obtain some insightful field expressions.

1) *Large Circular Loop on the Earth's Surface ( $h = 0$ ):* Assume that the static response is examined close to the Earth's surface ( $z \rightarrow 0$ ). With Wolfram Mathematica's online integration code [26], the right-hand side of (19) for  $h, z = 0$  can be expressed analytically, that is

$$\begin{aligned} \lim_{z \rightarrow 0} \int_0^\infty \lambda e^{-\lambda z} J_1(\lambda a) J_0(\lambda \rho) d\lambda \\ = \frac{2}{\pi a} \frac{1}{\sqrt{a^2 - \rho^2}} E \left[ \frac{\rho^2}{\rho^2 - a^2} \right] \end{aligned} \quad (20)$$

where  $E[x]$  is the complete elliptic integral of the second kind. Substituting (20) into (17), we have the vertical static response

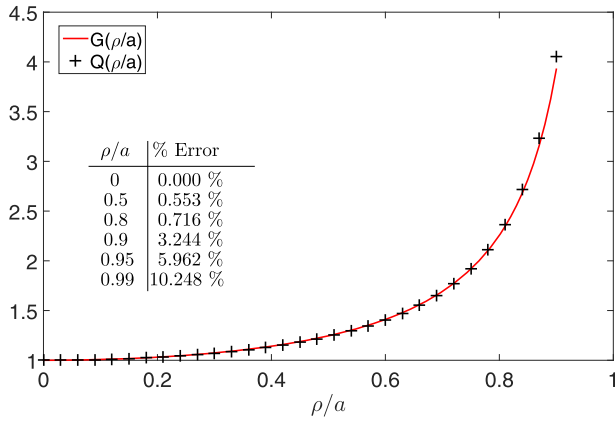


Fig. 1. Comparison between  $G(\rho/a)$  and its approximation  $Q(\rho/a)$ , for various values of  $\rho/a < 1$ . A % error for selected values is provided.

on the Earth's surface at radial distance  $\rho$  from the loop's center axis

$$\begin{aligned}
 B_z^{(0)}(\rho, 0) &= \frac{\mu_0 I}{\pi} \left( \frac{\Delta\chi}{2 + \Delta\chi} \right) \frac{1}{\sqrt{a^2 - \rho^2}} E \left[ \frac{\rho^2}{\rho^2 - a^2} \right] \\
 &= B_z^{(0)}(0, 0) \left( \frac{2}{\pi \sqrt{1 - (\rho/a)^2}} E \left[ \frac{(\rho/a)^2}{(\rho/a)^2 - 1} \right] \right) \\
 &= B_z^{(0)}(0, 0) G \left( \frac{\rho}{a} \right) \quad (21)
 \end{aligned}$$

where  $B_z^{(0)}(0, 0)$  represents the static magnetic response of the SP half-space at the loop's center, and  $G$  is a function that depends explicitly on  $(\rho/a)$ .

For measurements inside the loop ( $\rho < a$ ), we would like to find an approximate solution for  $G$  that does not contain the elliptic integral. At the center of the loop,  $\rho/a = 0$  and  $E[0] = \pi/2$ , (21) then simplifies to  $B_z^{(0)}(0, 0)$  as expected. As  $\rho \rightarrow a$ , the static response approaches infinity. To preserve these properties, we suggest an empirical function  $Q$  as

$$G \left( \frac{\rho}{a} \right) \approx Q \left( \frac{\rho}{a} \right) = 1 + \frac{9}{4\pi} \left( \frac{(\rho/a)^2}{1 - (\rho/a)^2} \right) \quad \text{for } \rho < a. \quad (22)$$

This approximation is accurate to within 1% for values  $\rho/a \leq 0.8$ . For  $\rho/a > 0.8$ , the approximation increasingly overestimates  $Q(\rho/a)$  (Fig. 1).

Combining (21) with (22), we have the analytical formula for the vertical static response at any location ( $\rho < a, z = 0$ ) for a loop located on the Earth surface ( $h = 0$ )

$$B_z^{(0)}(\rho, 0) \approx \frac{\mu_0 I}{2a} \left( \frac{\Delta\chi}{2 + \Delta\chi} \right) \left[ 1 + \frac{9}{4\pi} \left( \frac{(\rho/a)^2}{1 - (\rho/a)^2} \right) \right]. \quad (23)$$

## 2) Response Along the Transmitter's Vertical Axis ( $\rho = 0$ ):

When the transmitter loop is at height  $h$  and the observation is along the vertical axis of the transmitter, i.e., at  $(\rho = 0, z)$ , the associated integral in (19) is reduced to an analytical

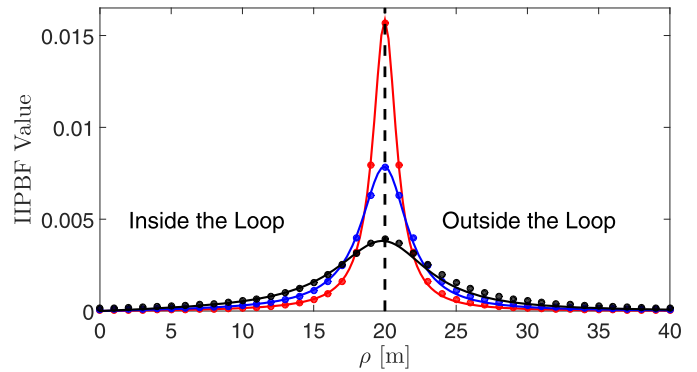


Fig. 2. Comparison between computations of the Hankel transform using IIPBF adaptive quadrature and using the empirical expression from (27). Comparisons are done for various values of  $0 < z + h \leq a/5$ , using a loop radius of  $a = 20$  m.

expression by setting  $\rho \rightarrow 0$

$$\lim_{\rho \rightarrow 0} \int_0^\infty \lambda e^{-\lambda(z+h)} J_1(\lambda a) J_0(\lambda \rho) d\lambda = a \left( \frac{1}{(z+h)^2 + a^2} \right)^{3/2}. \quad (24)$$

Substituting (24) into (17) leads to the vertical static response

$$B_z^{(0)}(0, z) = \frac{\mu_0 m}{2\pi} \left( \frac{\Delta\chi}{2 + \Delta\chi} \right) \left( \frac{1}{(z+h)^2 + a^2} \right)^{3/2} \quad (25)$$

where  $m = \pi a^2 I$  is the dipole moment of the transmitter.

## B. Radial Static Response for a Large Circular Transmitter Loop Over an SP Half-Space

Now, we look at the radial static response from a circular transmitter loop over an SP half-space. According to (18), we require a solution to the integral

$$\int_0^\infty \lambda e^{-\lambda(z+h)} J_1(\lambda a) J_1(\lambda \rho) d\lambda. \quad (26)$$

Although analytic solutions for (26) exist [25], they are too complicated to develop straightforward relationships with respect to the transmitter loop radius and observation locations. However, for the special cases considered in the following, we can have an approximate solution.

First, let us examine the behavior of (26). For  $z+h > 0$ , we used the IIPBF adaptive quadrature package [28] to evaluate the expression. Fig. 2 shows the results for several values of  $z+h$  for a loop of radius  $a = 20$  m. We observed that for  $0 < z+h \leq a/5$ , the numerical solutions with respect to  $\rho$  behaved like a Cauchy distribution centered around  $\rho = a$ . As  $z+h$  is decreased over the accepted range, the distribution became narrow. Therefore, invoking the probability density function for a Cauchy distribution, we proposed a heuristic approximation to (26) as

$$\int_0^\infty \lambda e^{-\lambda(z+h)} J_1(\lambda a) J_0(\lambda \rho) d\lambda \sim \left[ \pi a \gamma \left( 1 + \left( \frac{\rho - a}{\gamma} \right)^2 \right) \right]^{-1} \quad (27)$$

where an empirical function for  $\gamma$  is given by

$$\gamma = 2(z+h) \left( \frac{2}{\pi} \right)^{3/2}. \quad (28)$$

One sees that in Fig. 2, the results from (27) match well with those using IIPBF adaptive quadrature. For  $z+h \rightarrow 0$ , (26) approaches the Dirac delta function  $\delta(x)$

$$\lim_{z+h \rightarrow 0} \int_0^\infty \lambda e^{-\lambda(z+h)} J_1(\lambda a) J_1(\lambda \rho) d\lambda = \frac{\delta(a-\rho)}{a} \quad (29)$$

which can be shown with the weighted orthogonality property of the Hankel transform [27].

By combining (18) and (27), the radial static response of the SP half-space for  $0 < z+h \leq a/5$  is approximated by

$$B_\rho^{(0)}(\rho, z) \sim -\frac{\mu_0 I}{2} \left( \frac{\Delta\chi}{2 + \Delta\chi} \right) \left[ \pi a \gamma \left( 1 + \left( \frac{\rho-a}{\gamma} \right)^2 \right) \right]^{-1}. \quad (30)$$

It should be noted that although (30) provides a reasonable approximation, it cannot be used to show that  $B_\rho^{(0)}(\rho \rightarrow 0, z) = 0$  exactly. This property was obtained from (18), since  $J_1(0) = 0$ .

## V. VRM RESPONSE FROM A LARGE CIRCULAR TRANSMITTER LOOP

Having obtained the approximations for the aftereffect function and the analytical expressions for the static fields in several cases, we now look at the VRM response with (15) and (16) over an SP half-space for  $\tau_1 \ll t \ll \tau_2$ .

### A. Vertical VRM Response From a Large Circular Transmitter Loop

1) *Large Circular Loop on the Earth's Surface ( $h = 0$ ):* With expressions (11) and (23), the vertical VRM response at any location ( $\rho < a, z = 0$ ) at time  $\tau_1 \ll t \ll \tau_2$  is approximated according to (15)

$$B_z(\rho, 0, t) \approx \frac{\mu_0 I}{2a} \left( \frac{\Delta\chi}{2 + \Delta\chi} \right) \left[ 1 + \frac{9}{4\pi} \left( \frac{(\frac{\rho}{a})^2}{1 - (\frac{\rho}{a})^2} \right) \right] \bar{F}(t). \quad (31)$$

Similarly, after the substitution of (13) and (23) into (16), we have

$$\frac{\partial B_z(\rho, 0, t)}{\partial t} \approx \frac{\mu_0 I}{2a} \left( \frac{\Delta\chi}{2 + \Delta\chi} \right) \left[ 1 + \frac{9}{4\pi} \left( \frac{(\frac{\rho}{a})^2}{1 - (\frac{\rho}{a})^2} \right) \right] \frac{d\bar{F}(t)}{dt}. \quad (32)$$

Both (31) and (32) reveal that the vertical VRM response depends upon the ratio of  $\rho/a$ . When an observation is made toward the center of a loop (say  $\rho/a \leq 0.5$ ), the response tends to be small and vary minimally with respect to  $\rho$ . This agrees with the results obtained by others [1], [2]. When an observation is made toward the edges of the loop, the VRM response can increase in magnitude rapidly as  $\rho$  increases and  $\rho/a \rightarrow 1$ . Fig. 3 shows the variation in the VRM response when  $\rho = 0, 10,$  and  $18$  m for a loop of radius  $a = 20$  m.

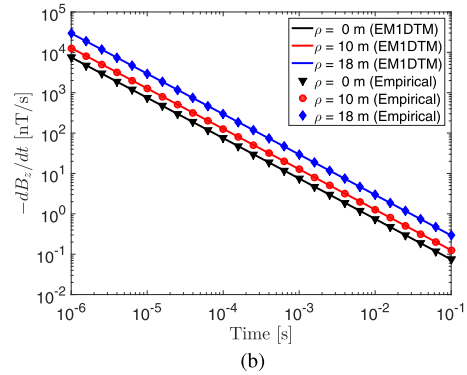
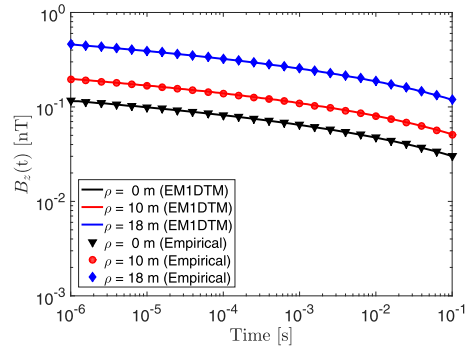


Fig. 3. Vertical VRM response for a large circular loop of radius  $a = 20$  m on the Earth's surface, at radial distance  $\rho$  from the loop's center, using properties  $\Delta\chi = 0.01$ ,  $\tau_1 = 10^{-8}$  s, and  $\tau_2 = 10$  s. This plot compares expressions (31) and (32) to values obtained using the EM1DTM code. (a)  $B_z(t)$ . (b)  $-\partial B_z/\partial t$ .

Meanwhile, the results of (31) and (32) match well with those computed using the 1-D numerical code-EM1DTM [18]. In practice, measurements of  $B$  or  $\partial B/\partial t$  are not acquired directly on the Earth's surface. Instead, data are typically collected at heights less than 1 m off the ground. Therefore, for a near-surface survey with a sufficiently large loop, we should expect similar behavior to the case mentioned earlier when  $a \gg z$ .

2) *Response Along the Transmitter's Vertical Axis ( $\rho = 0$ ):* Using expressions (11), (15), and (25), we have the VRM response at time  $\tau_1 \ll t \ll \tau_2$

$$B_z(0, z, t) \approx \frac{\mu_0 m}{2\pi} \left( \frac{\Delta\chi}{2 + \Delta\chi} \right) \left( \frac{1}{(z+h)^2 + a^2} \right)^{3/2} \bar{F}(t). \quad (33)$$

Similarly, using expressions (13), (15), and (25), we obtain

$$\frac{\partial B_z(0, z, t)}{\partial t} \approx \frac{\mu_0 m}{2\pi} \left( \frac{\Delta\chi}{2 + \Delta\chi} \right) \left( \frac{1}{(z+h)^2 + a^2} \right)^{3/2} \frac{d\bar{F}(t)}{dt}. \quad (34)$$

Equations (33) and (34) show that the VRM response becomes smaller in magnitude when the size of the loop or the total elevation of  $z+h$  increases. This matches analytic results and field observations made by others [1], [2], [11]. For a dipole source ( $a \ll z+h$ ), the magnitude of the VRM response is proportional to  $(z+h)^{-3}$ . For  $z+h = 0$  and  $m = \pi a^2 I$ ,

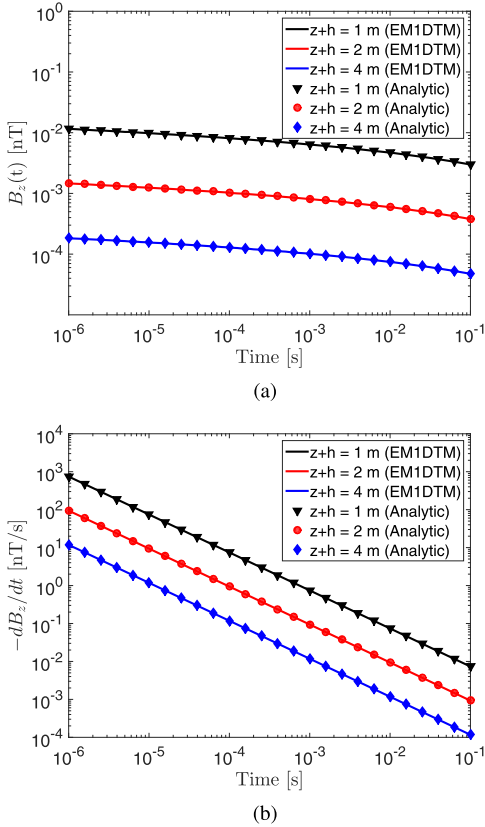


Fig. 4. Vertical VRM response along the transmitters vertical axis of symmetry, using a radius of  $a = 0.2$  m. Responses were predicted for several values  $z + h$ , using properties  $\Delta\chi = 0.01$ ,  $\tau_1 = 10^{-8}$  s, and  $\tau_2 = 10$  s. Plots compare (33) and (34) to values obtained using the EM1DTM code. (a)  $B_z(t)$ . (b)  $-\partial B_z/\partial t$ .

expressions (33) and (34) are equivalent to expressions (31) and (32) at  $\rho = 0$ . The VRM response observed for a loop of radius  $a = 0.2$  m is shown in Fig. 4 when  $z + h = 1, 2$ , and 4 m. Again, both the analytical and numerical results agree well.

### B. Radial VRM Response From a Large Circular Transmitter Loop

Using (11), (15), and (30), we express the radial VRM response for  $0 < z + h \leq a/5$  at time  $\tau_1 \ll t \ll \tau_2$  as

$$B_\rho(\rho, z, t) \sim -\frac{\mu_0 I}{2} \left( \frac{\Delta\chi}{2 + \Delta\chi} \right) \times \left[ \pi a \gamma \left( 1 + \left( \frac{\rho - a}{\gamma} \right)^2 \right) \right]^{-1} \bar{F}(t). \quad (35)$$

And using expressions (13), (15), and (30), we have

$$\frac{\partial B_\rho(\rho, z, t)}{\partial t} \sim -\frac{\mu_0 I}{2} \left( \frac{\Delta\chi}{2 + \Delta\chi} \right) \times \left[ \pi a \gamma \left( 1 + \left( \frac{\rho - a}{\gamma} \right)^2 \right) \right]^{-1} \frac{d\bar{F}}{dt}. \quad (36)$$

Equations (35) and (36) describe how the geometrical parameters can affect the response, although they are a bit more complicated than the expressions for the vertical component.

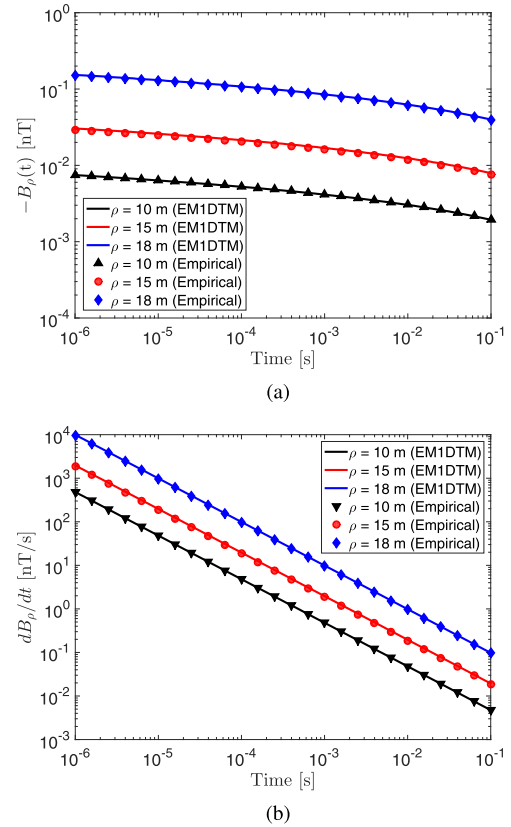


Fig. 5. Comparison between EM1DTM and empirical functions (35) and (36) for the radial VRM response with a loop of radius  $a = 20$  m. The response was predicted for  $z + h = 20$  m using physical properties  $\Delta\chi = 0.01$ ,  $\tau_1 = 10^{-8}$  s, and  $\tau_2 = 10$  s. (a)  $-B_\rho(t)$ . (b)  $dB_\rho/dt$ .

Near the center of the loop, one can see that the radial component of the VRM response is small. As observations are made closer to the transmitter wire, the radial component of the VRM response increases significantly. Recall that  $\gamma$  given by (28) is a function of  $z + h$ . Therefore, the effect of raising the receiver off the ground can be generated by raising the transmitter off the ground. This effect was observed during field observations for various SiroTEM configurations [1].

Fig. 5(a) and (b) shows the radial VRM response for  $\rho = 10, 15$ , and 18 m given a loop of radius  $a = 20$  m and  $z + h = 1$  m. The analytical and the EM1DTM results overlap well. Similar to the vertical components, the VRM response of  $B_\rho(t)$  decays in  $\ln(t)$ , and  $\partial B_\rho/\partial t$  decays in  $1/t$ .

## VI. RESPONSE OVER A CONDUCTIVE AND MAGNETICALLY VISCOUS HALF-SPACE

The magnetic susceptibilities of lateritic soils are generally low ( $\chi < 0.01$ ) [15], [29], [30]; as such, the magnetic properties of lateritic soils do not have a significant impact on the inductive response. Some studies showed that effects of conductivity may be neglected when considering the soil's VRM response [3], [14], [15]. Some have suggested that the inductive and VRM responses from lateritic soils are approximately separable [1], [4], [14]. In this section, we will test this assumption using the 1-D numerical modeling

code (EM1DTM) [18] over a half-space model. Given that the inductive and VRM responses are separable, we present the critical time analysis by comparing the vertical inductive and VRM responses with respect to the loop's radius and observation distances.

### A. Separation of Inductive and VRM Responses

Consider a conductive and magnetically viscous half-space with  $\sigma = 0.01$  S/m,  $\chi_\infty = 0$ ,  $\Delta\chi = 0.001$ ,  $\tau_1 = 10^{-8}$  s, and  $\tau_2 = 10$  s. Fig. 6 shows the inductive, the VRM, and the total transient responses computed by EM1DTM for a loop of radius  $a = 20$  m on the surface. One sees that for the vertical and radial components after sufficient time, the observed response becomes dominated by the VRM response, whereas the early times appear to be dominated by the inductive response. The numerical results verify that the total response for a conductive and magnetically viscous Earth can be well approximated as the sum of the individual inductive and VRM responses and support the observations made by [1], [3], [4], [14], [15], [29], and [30]. Overall, we found that for sufficiently small dc susceptibilities ( $\chi_\infty + \Delta\chi < 0.01$ ), inductive and VRM responses could be predicted independently. For larger values of  $\chi_\infty + \Delta\chi$ , magnetic properties can affect the inductive response. On the other hand, the VRM response was insensitive to changes to the half-space conductivity. Bear in mind that the value of  $\chi_\infty$  has no effect on the VRM response as the contribution made by instantaneous magnetization during the off-time is zero.

### B. Estimating the Crossover Time of VRM Responses

Nabighian [17] showed that for a step-off excitation, to the first-order, the quasi-static inductive response within a large circular transmitter loop on the surface of a conductive half-space would approach the following expression asymptotically after sufficient time:

$$B_z(t) \approx \frac{I\sigma^{3/2}\mu_0^{5/2}a^2}{30\sqrt{\pi}}t^{-3/2} \quad (37)$$

and that

$$\frac{\partial B_z}{\partial t} \approx -\frac{I\sigma^{3/2}\mu_0^{5/2}a^2}{20\sqrt{\pi}}t^{-5/2} \quad (38)$$

where  $a$  is the loop's radius,  $\sigma$  is the Earth's conductivity, and  $\mu_0$  is the permeability of free space. Note the inductive response and its derivative decay according to  $t^{-3/2}$  and  $t^{-5/2}$ , respectively. Furthermore, the strength of the inductive response is proportional to  $a^2$ .

As the inductive and VRM responses can be predicted independently, we want to inspect how both responses change over time. Refer to Fig. 6. We observe that the decay rate of the total response starts to change roughly at a time when the inductive curve intersects with the VRM curve. Thus, by setting up the ratio between the vertical inductive response  $B_z^{(IND)}$  and the vertical VRM response  $B_z^{(VRM)}$  with (11),

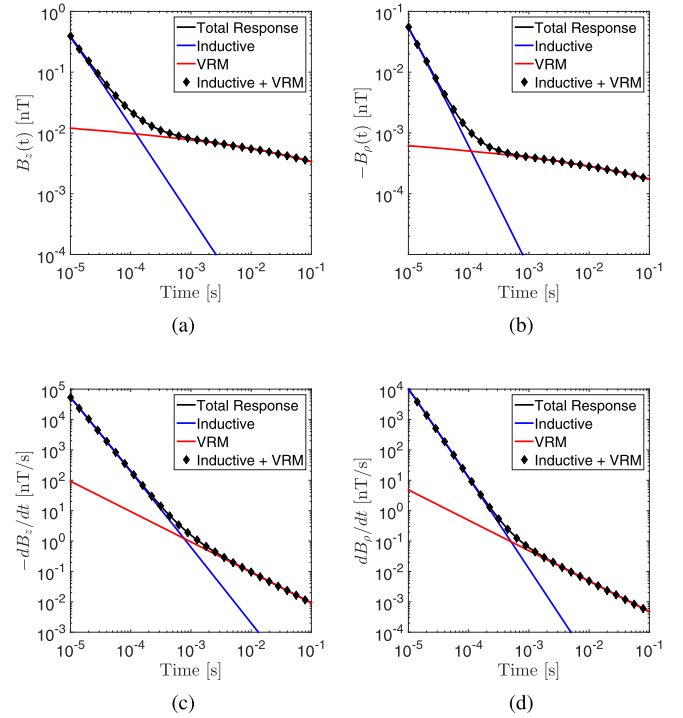


Fig. 6. Additivity of the inductive and VRM responses for a loop of radius  $a = 20$  m at location  $(\rho, z) = (10 \text{ m}, 1 \text{ m})$ . The half-space was given physical properties:  $\sigma = 0.01$  S/m,  $\chi_\infty = 0$ ,  $\Delta\chi = 0.001$ ,  $\tau_1 = 10^{-8}$  s, and  $\tau_2 = 10$  s. (a)  $B_z(t)$ . (b)  $-B_\rho(t)$ . (c)  $-\partial B_z/\partial t$ . (d)  $\partial B_\rho/\partial t$ .

(31), and (37)

$$R_B = \frac{B_z^{(IND)}}{B_z^{(VRM)}} \approx \frac{\ln(\tau_2/\tau_1)}{15 Q(\rho/a)\sqrt{\pi}} \left( \frac{2 + \Delta\chi}{\Delta\chi} \right) \times \left( \frac{t^{-3/2}}{-\gamma - \ln(t/\tau_2)} \right) (\mu_0\sigma)^{3/2} a^3 \quad (39)$$

and for the derivative with (13), (32), and (38)

$$R_{dB/dt} = \frac{\partial B_z/\partial t^{(IND)}}{\partial B_z/\partial t^{(VRM)}} \approx \frac{\ln(\tau_2/\tau_1)}{10 Q(\rho/a)\sqrt{\pi}} \left( \frac{2 + \Delta\chi}{\Delta\chi} \right) (\mu_0\sigma)^{3/2} a^3 t^{-3/2} \quad (40)$$

we can estimate the time at which magnetic viscosity begins to dominate the vertical observed response. Such times are called the crossover time. Let  $t_\alpha$  denote the crossover time for  $B_z$ , which solves  $R_B = 1$  in (39). And let  $t_\beta$  denote the crossover time for  $\partial B_z/\partial t$ , which solves  $R_{dB/dt} = 1$  in (40). For  $\partial B_z/\partial t$ , the crossover time  $t_\beta$  is straightforward

$$t_\beta \approx \left[ \frac{\ln(\tau_2/\tau_1)}{10 Q(\rho/a)\sqrt{\pi}} \left( \frac{2 + \Delta\chi}{\Delta\chi} \right) \right]^{2/3} \mu_0\sigma a^2. \quad (41)$$

Equation (41) states that by increasing the radius of a transmitter loop, the expected time  $t_\beta$  at which  $\partial B_z/\partial t$  becomes dominated by the VRM response is pushed to a later time. At the center of any loop,  $Q = 1$  and  $t_\beta \propto \sigma a^2$ . Because  $t_\beta \propto Q^{-2/3}$ , as an observation moves toward the edge of the

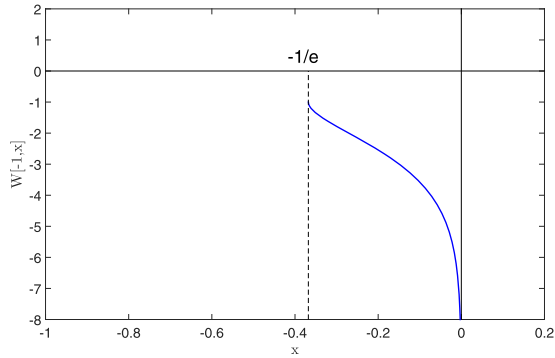


Fig. 7. Lower branch of the Lambert W function  $W[-1, x]$  for values  $-1/e \leq x \leq 0$ .

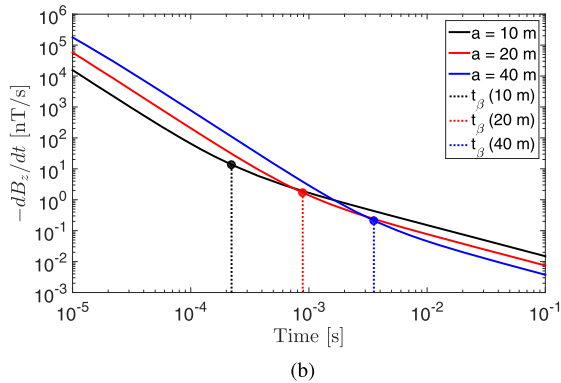
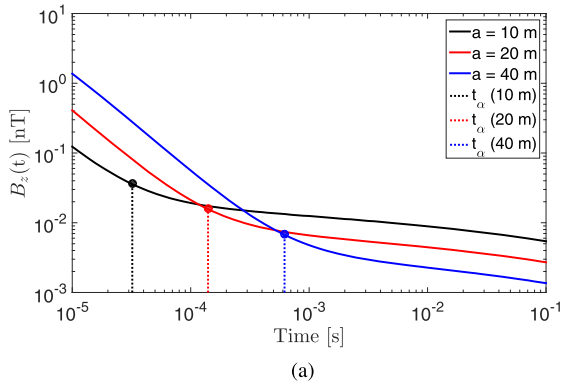


Fig. 8. Vertical transient response at the center of a set of transmitter loops with varying radii, located on the Earth's surface. EM1DTM was used to predict the responses for a half-space with physical properties:  $\sigma = 10^{-2}$  S/m,  $\Delta\chi = 0.001$ ,  $\tau_1 = 10^{-8}$  s, and  $\tau_2 = 10$  s. (a)  $B_z(t)$ . (b)  $-\partial B_z/\partial t$ .

loop, we expect  $t_\beta$  to decrease, and thus, the VRM response starts to dominate earlier.

For  $B_z(t)$ , the VRM response begins to dominate at time

$$t_\alpha \approx t_\beta \left( -W \left[ -1, -\left( \frac{t_\beta}{\tau_2} e^\gamma \right)^{3/2} \right] \right)^{-2/3} \leq t_\beta \quad (42)$$

where  $W[-1, x]$  is the lower branch of the Lambert W function [31],  $\gamma = 0.5772$  is the Euler constant, and  $t_\beta$  is given in (41).  $W[-1, x]$  for values  $-1/e \leq x \leq 0$  is shown in Fig. 7. Its derivation can be found in the Appendix.

Equation (42) shows that  $t_\alpha$  is a monotonic increasing function with respect to  $t_\beta$ . Although the dependence of  $t_\alpha$  on  $a$  and  $Q(\rho/a)$  is not straightforwardly represented

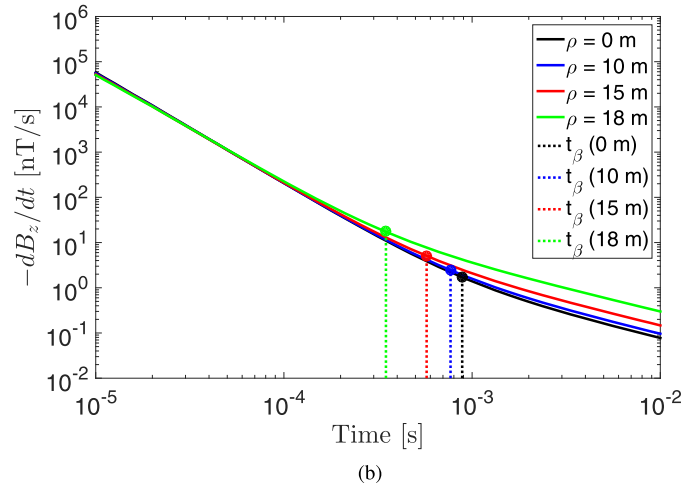
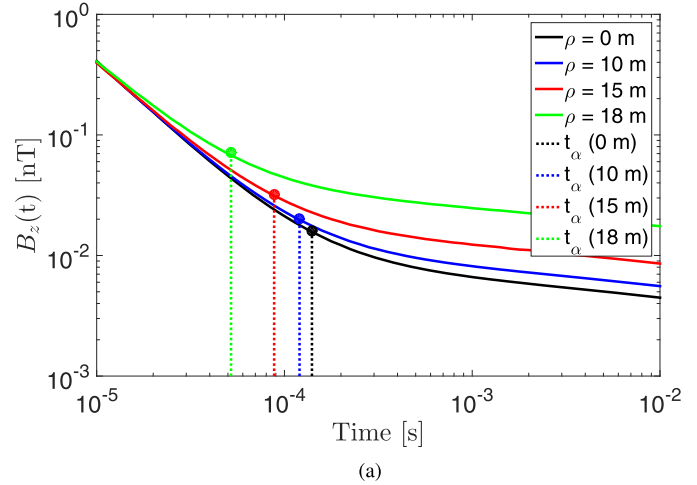


Fig. 9. Vertical transient response at off-axis locations  $\rho$ , for a loop of radius  $a = 20$  m, located on the Earth's surface. EM1DTM was used to predict the responses for a half-space with physical properties:  $\sigma = 10^{-2}$  S/m,  $\Delta\chi = 0.001$ ,  $\tau_1 = 10^{-8}$  s, and  $\tau_2 = 10$  s. (a)  $B_z(t)$ . (b)  $-\partial B_z/\partial t$ .

in (42), we can qualitatively infer that TEM instruments, which measure  $B_z(t)$ , are much more affected by the VRM response than instruments, which measure  $\partial B_z/\partial t$ . It can be shown that  $t_\alpha \ll t_\beta$  for  $t_\beta \ll \tau_2 e^\gamma$ . Fig. 8 shows the vertical transient responses calculated using the EM1DTM at the center of a transmitter loop when the radius  $a = 10, 20$ , and  $40$  m.  $t_\alpha$  and its corresponding value  $B_z(t)$  were calculated using (11), (31), (37), and (42);  $t_\beta$  and its corresponding value  $\partial B_z/\partial t$  were calculated using (13), (32), (38), and (41). It confirms that  $t_\alpha$  and  $t_\beta$  increase with respect to  $a$ , and that  $t_\alpha \leq t_\beta$ .

Consider the vertical transient responses in Fig. 9 at various radial locations  $\rho$  for a transmitter loop with radius  $a = 20$  m.  $t_\alpha$  and its corresponding value  $B_z(t)$  were calculated using (11), (31), (37), and (42);  $t_\beta$  and its corresponding value  $\partial B_z/\partial t$  were calculated using (13), (32), (38), and (41). Similarly, we observe that  $t_\alpha$  and  $t_\beta$  decrease with respect to  $\rho$ , and that  $t_\alpha \leq t_\beta$ . Recall that  $Q$  in (22) increases as  $\rho \rightarrow a$ . Thus, when observations are made closer to the transmitter loop, the VRM response will not only increase but will also dominate the total observed transient response at earlier times. This is consistent with the observation that

magnetic viscosity is known to be most problematic near the transmitter wire [1], [2], [11].

Figs. 8 and 9 demonstrate how (41) and (42) can be used to estimate the crossover times (dashed lines) at which  $B_z(t)$  and  $\partial B_z/\partial t$  within the loop become dominated by the VRM response. The projection of  $t_\alpha$  and  $t_\beta$  on the corresponding total response curve will appear earlier than the point of maximum curvature on each log–log plot (also see Fig. 6). Provided that *a-priori* information is supplied regarding the Earth’s physical properties, (39)–(42) can provide some survey guides in practice. For example, (39) and (40) can be used to help adjust a loop size that renders the VRM response negligible over a specified time range. With an estimated crossover time, one can properly remove the VRM effects during the late-time response.

## VII. CONCLUSION

In this paper, we have presented the analytical formulas for the transient VRM response generated by a large circular loop over a magnetically viscous half-space for a step-off excitation. Assuming that the soil’s magnetic viscosity is represented by a collection of noninteracting SP grains [7] and that magnetic fields are governed by the magnetostatic law, we can express the VRM response and its derivatives as the product of a static field and an aftereffect time function. We approximated the true aftereffect function of the half-space by using a log-uniform distribution of time-relaxation constants to characterize the magnetic viscosity. As for the static fields, we derived the associated expressions by simplifying and approximating Hankel integrals for the vertical and radial field components. Analytic expressions were verified with the 1-D forward modeling code [18]. Both analytical and numerical results showed excellent agreement for sufficiently small magnetic susceptibilities.

Our analytic expressions explicitly reveal how the VRM response depends upon geometric survey properties, such as the transmitter loop’s size and the observation location within the loop. For vertical VRM responses measured near the surface, the ratio of  $\rho/a$  plays a major role in controlling the magnitude. When  $\rho/a \rightarrow 1$ , i.e., an observation is made toward the edge of the loop, VRM responses can increase significantly. Equivalently, strong VRM responses are expected for smaller transmitter loops. For measurements along the axis of the loop, the vertical VRM response can be diminished by either increasing the sensor height or increasing the size of the loop. For radial VRM responses, our empirical approximation predicts that it is small near the center of the loop. As observations are made closer to the transmitter wire, the increased strength of radial VRM response can be damped by increasing the sensor height. Characteristics of the VRM response uncovered in the analytical expressions are consistent with other field observations and numerical modeling results [1]–[5], [13].

Furthermore, we have suggested an estimate of the crossover time from which the response might be divided into early inductive and late VRM stages. Increasing the size of a loop can push the crossover time to a later time. On the other hand,

a near loop-edge observation tends to have an early crossover time. Also, we found that the VRM response impacts on the magnetic flux density  $B(t)$  at much earlier times than on its time derivative  $dB/dt$ . Therefore, in regions where lateritic soils are prominent, it may not be recommended to use TEM systems that only measure the magnetic flux density, which are potentially contaminated by the VRM signal across a larger number of time channels.

Overall, our analytical expressions can serve as a convenient design code for choosing an appropriate loop size and selecting an optimal range of observation times. This may prove beneficial when attempting to reduce the VRM response or pinpoint a certain time window where the VRM response can be properly removed.

## APPENDIX

We wish to solve expression (39) for  $R_B = 1$  to obtain expression (42). This is equivalent to solving an expression of the form

$$At^{-3/2} + \ln t \approx -\gamma + \ln \tau_2 \quad (\text{A1})$$

where

$$A = \frac{\ln(\tau_2/\tau_1)}{15 Q(\rho/a)\sqrt{\pi}} \left( \frac{2 + \Delta\chi}{\Delta\chi} \right) (\mu_0\sigma)^{3/2} a^3. \quad (\text{A2})$$

Changing the variable  $u = t^{-3/2}$ , and with some algebra, we can rewrite (A1) as

$$-\frac{3}{2} A u e^{-\frac{3}{2} A u} \approx -\frac{3}{2} A e^{\frac{3}{2}(\gamma - \ln \tau_2)}. \quad (\text{A3})$$

Solutions to an expression of the form  $x e^x = C$  are defined as branches of the Lambert W function  $W[n, C]$ , where  $n$  values are integer values [31]. Therefore, the solutions  $u_n$  to (A3) are

$$u_n \approx -\frac{2}{3A} W \left[ n, -\frac{3}{2} A e^{\frac{3}{2}(\gamma - \ln \tau_2)} \right]. \quad (\text{A4})$$

We can use (41) and (A2) to show  $A = \frac{2}{3} t_\beta^{3/2}$ . By replacing  $u_n = t_n^{-3/2}$

$$\begin{aligned} t_n^{-3/2} &\approx -t_\beta^{-3/2} W \left[ n, -t_\beta^{3/2} e^{\frac{3}{2}(\gamma - \ln \tau_2)} \right] \\ \implies t_n &\approx t_\beta \left( -W \left[ n, -\left( \frac{t_\beta}{\tau_2} e^\gamma \right)^{3/2} \right] \right)^{-2/3}. \end{aligned} \quad (\text{A5})$$

Real-valued solutions  $W[n, x]$  only exist for  $n = -1, 0$  [31]. In addition, for  $t_n$  to occur after the primary field has been removed ( $t_n \geq 0$ ),  $W[n, x]$  requires  $-1/e \leq x \leq 0$ . Thus, by (A5)

$$\begin{aligned} -1/e &\leq -\left( \frac{t_\beta}{\tau_2} e^\gamma \right)^{3/2} \leq 0 \\ \implies e^{-\frac{2}{3}\gamma} &\approx 0.288267 \geq \frac{t_\beta}{\tau_2} \geq 0. \end{aligned} \quad (\text{A6})$$

Recall that our choice in aftereffect function (11) is only valid for  $\tau_1 \ll t \ll \tau_2$ . Therefore, the condition defined in expression (A6) is reasonable under the assumption that  $t_\beta \ll \tau_2$ . We evaluated (A5) for  $n = 0$  and noticed the solutions were  $t_0 \ll \tau_2$ . This violates our conditions for the aftereffect function and is, therefore, not a valid solution.

On the other hand, solutions of (A5) for  $n = -1$  did not violate conditions for the aftereffect function. The solutions obtained using  $W[-1, x]$  consistently showed  $t_\alpha \leq t_\beta$ . As a result, the time  $t_\alpha$ , which solves  $R_B = 1$  in expression (39) is given by

$$t_\alpha \approx t_\beta \left( -W \left[ -1, -\left( \frac{t_\beta}{\tau_2} e^\gamma \right)^{3/2} \right] \right)^{-2/3} \leq t_\beta. \quad (\text{A7})$$

## REFERENCES

- [1] G. Buselli, "The effect of near-surface superparamagnetic material on electromagnetic measurements," *Geophysics*, vol. 47, no. 9, pp. 1315–1324, Sep. 1982.
- [2] P. O. Barsukov and E. B. Fainberg, "Superparamagnetic effect over gold and nickel deposits," *Eur. J. Environ. Eng. Geophys.*, vol. 6, pp. 61–72, Feb. 2001.
- [3] S. D. Billings, L. R. Pasion, D. W. Oldenburg, and J. Foley, "The influence of magnetic viscosity on electromagnetic sensors," in *Proc. Int. Conf. Requirements and Technol. for the Detection, Removal and Neutralization of Landmines UXO*, vol. 1, H. Sahli, A. M. Bottoms, and J. Cornelius, Eds. Brussels, Belgium, Sep. 2003, pp. 123–130.
- [4] L. R. Pasion, "Inversion of time domain electromagnetic data for the detection of unexploded ordnance," Ph.D. dissertation, Dept. Geophys., Univ. British Columbia, Vancouver, BC, Canada, 2007.
- [5] V. Y. Zadorozhnaya, N. O. Kozhevnikov, and P. Nyabeze, "Superparamagnetic effect, effect provided by 'red soil' in Southern Africa," in *Proc. 21st EM Induction Workshop*, Darwin, Australia, Jul. 2012, pp. 1–4.
- [6] M. Dabas, A. Jolivet, and A. Tabbagh, "Magnetic susceptibility and viscosity of soils in a weak time varying field," *Geophys. J. Int.*, vol. 108, no. 1, pp. 101–109, 1992.
- [7] P. M. L. Néel, "Théorie du traînage magnétique des ferromagnétiques en grains fins avec application au terres cuites," *Ann. Geophys.*, vol. 5, pp. 99–136, 1949.
- [8] B. M. Moskowitz, "Magnetic viscosity, diffusion after-effect, and disaccommodation in natural and synthetic samples," *Geophys. J. Int.*, vol. 82, no. 2, pp. 143–161, 1985.
- [9] D. K. Butler, "Implications of magnetic backgrounds for unexploded ordnance detection," *J. Appl. Geophys.*, vol. 54, pp. 111–125, Nov. 2003.
- [10] Y. Das, "A preliminary investigation of the effects of soil electromagnetic properties on metal detectors," in *Proc. SPIE Conf. Detect. Remediation Technol. Mines Mine-Like Targets IX*, vol. 5415. Orlando, FL, USA, Apr. 2004, pp. 677–690.
- [11] T. Lee, "The effect of a superparamagnetic layer on the transient electromagnetic response of a ground," *Geophys. Prospecting*, vol. 32, no. 3, pp. 480–496, 1984.
- [12] L. R. Pasion, S. D. Billings, and D. W. Oldenburg, "Evaluating the effects of magnetic soils on TEM measurements for UXO detection," in *SEG Technical Program Expanded Abstracts*, 2002, pp. 1428–1431.
- [13] N. O. Kozhevnikov and E. Y. Antonov, "The magnetic relaxation effect on TEM responses of a uniform earth," *Russian Geol. Geophys.*, vol. 49, no. 3, pp. 197–205, 2007.
- [14] Y. Das, "Effects of soil electromagnetic properties on metal detectors," *IEEE Trans. Geosci. Remote Sens.*, vol. 44, no. 6, pp. 1444–1453, Jun. 2006.
- [15] P. Druyts, Y. Das, C. Craeye, and M. Acheroy, "Modeling the response of electromagnetic induction sensors to inhomogeneous magnetic soils with arbitrary relief," *IEEE Trans. Geosci. Remote Sens.*, vol. 47, no. 8, pp. 2627–2638, Aug. 2009.
- [16] P. G. Lelièvre and D. W. Oldenburg, "Magnetic forward modelling and inversion for high susceptibility," *Geophys. J. Int.*, vol. 166, no. 1, pp. 76–90, 2006.
- [17] M. N. Nabighian, "Quasi-static transient response of a conducting half-space—An approximate representation," *Geophysics*, vol. 44, no. 10, pp. 1700–1705, Oct. 1979.
- [18] C. G. Farquharson, "Background for program 'EM1DTM'," Geophys. Inversion Facility, Dept. Earth Ocean Sci., Univ. British Columbia (UBC-GIF), Vancouver, BC, Canada, Tech. Rep., Jun. 1, 2006.
- [19] P. C. Fannin and S. W. Charles, "On the influence of distribution functions on the after-effect function of ferrofluids," *J. Phys. D, Appl. Phys.*, vol. 28, no. 2, pp. 239–242, 1995.
- [20] C. E. Mullins and M. S. Tite, "Magnetic viscosity, quadrature susceptibility, and frequency dependence of susceptibility in single-domain assemblies of magnetite and maghemite," *J. Geophys. Res.*, vol. 78, no. 5, pp. 804–809, 1973.
- [21] H.-U. Worm, "On the superparamagnetic—Stable single domain transition for magnetite, and frequency dependence of susceptibility," *Geophys. J. Int.*, vol. 133, no. 1, pp. 201–206, 1998.
- [22] J. Igel, H. Preetz, and S. Altfelder, "Magnetic viscosity of tropical soils: Classification and prediction as an aid for landmine detection," *Geophys. J. Int.*, vol. 190, no. 2, pp. 843–855, 2012.
- [23] R. J. Blakely, "Magnetization," in *Potential Theory in Gravity and Magnetic Applications*, 1st ed. Cambridge, U.K.: Cambridge Univ. Press, 1996, ch. 5, sec. 5.1, pp. 82–83.
- [24] S. H. Ward and G. W. Hohmann, "Electromagnetic theory for geophysical applications," in *Electromagnetic Methods in Applied Geophysics*, vol. 1, M. N. Nabighian, Ed. Tulsa, OK, USA: Soc. of Exploration Geophysics, 1988.
- [25] H. Bateman, *Tables of Integral Transforms*, vol. 2. New York, NY, USA: McGraw-Hill, 1954.
- [26] Wolfram Research Inc. (2016). *Wolfram Mathematic Online Integrator*. [Online]. Available: <http://integrals.wolfram.com/index.jsp>
- [27] Y. T. Li and R. Wong, "Integral and series representations of the dirac delta function," *Commun. Pure Appl. Anal.*, vol. 7, no. 2, pp. 229–247, 2008.
- [28] J. T. Ratnanather, J. H. Kim, S. Zhang, A. M. J. Davis, and S. K. Lucas, "Algorithm 935: IIPBF, a MATLAB toolbox for infinite integral of products of two Bessel functions," *ACM Trans. Math. Softw.*, vol. 40, no. 2, Feb. 2014, Art. no. 14.
- [29] R. L. Van Dam *et al.*, "Spatial variability of magnetic soil properties," in *Proc. SPIE Conf. Detect. Remediation Technol. Mines Mine-Like Targets IX*, vol. 5415. Orlando, FL, USA, Apr. 2004, pp. 665–676.
- [30] R. L. Van Dam *et al.*, "Mineralogy of magnetic soils at a UXO remediation site in Kaho'olawe Hawaii," in *Proc. 18th Annu. Symp. Appl. Geophys. Eng. Environ. Problems*, Atlanta, GA, USA, Apr. 2005, pp. 666–677.
- [31] R. M. Corless, G. H. Gonnet, D. E. G. Hare, D. J. Jeffrey, and D. E. Knuth, "On the Lambert W function," *Adv. Comput. Math.*, vol. 5, no. 1, pp. 329–359, 1996.



**Devin C. Cowan** (S'16) received the B.Sc. degree in physics and earth sciences from the University of Victoria, Victoria, BC, Canada, in 2012 and the M.Sc. degree in geophysics from The University of British Columbia (UBC), Vancouver, BC, Canada, in 2016.

He was a Co-Op Student in 2012. He was with the Pacific Geoscience Centre, Sidney, BC, Canada, where he was involved in the study of physical rock properties. He then joined the UBC Geophysical Inversion Facility (UBC-GIF), where he is currently a member, with a focus on research VRM responses and their impact on mineral exploration and unexploded ordnance remediation. He has been heavily involved in developing EM GeoSci, an online learning resource for electromagnetic geophysics. His research interests include 3D forward modeling and inversion of viscous remanent magnetization responses.

**Lin-Ping Song** (M'06), photograph and biography not available at the time of publication.

**Douglas W. Oldenburg**, photograph and biography not available at the time of publication.